REVIEWS OF GEOPHYSICS, VOL. 23, NO. 1, PAGES 49–60, FEBRUARY 1985

Acoustic Properties of Sediments: An Update

LOYD HAMPTON

Applied Research Laboratories, The University of Texas at Austin, Austin, Texas

This paper will summarize our knowledge of the propagation of sound in marine sediments. This knowledge is important to a wide range of acoustic problems, extending from the high-frequency applications of detection of objects buried in the bottom sediment to the very low frequency application characterizing the propagation of acoustic energy over hundreds of kilometers. In these applications the ocean bottom becomes an important part of the acoustic waveguide. The desirable goal of a complete theoretical understanding of propagation has not been achieved. However, recent measurements of acoustic attenuation in the frequency range of a few hundred hertz are almost an order of magnitude smaller than have previously been measured, and these results may now permit progress in a more complete characterization of the acoustic properties of sediments. (The research performed on this topic by the author under the guidance of R. Reid was published in 1967 ("Acoustic Properties of Sediments," *J. Acoust. Soc. Am.*, *42*, 882–890, 1967). This paper will briefly review aspects of that work and trace the progress in this area of research since that publication.)

INTRODUCTION

Exploitation of the useful properties of sound in the ocean advanced with advances in several technologies, especially transducer development and the related electronics. Each new application broadened our fundamental knowledge of the acoustic properties of the medium. As an example, measurements of attenuation in the 1950's revealed the relaxation phenomenon due to the magnesium sulphate ion between about 60 kHz and 1 MHz. These measurements were made in the laboratory. Within the past few years the relaxation effects of the boron ions have been examined in the 100-Hz to 1-kHz region. Because attenuation values are quite small, i.e., two orders of magnitude smaller than the effects of magnesium sulphate, these measurements require extracting results from both laboratory and in situ measurements. Currently, there is a controversy concerning acoustic attenuation mechanisms in the ocean near the frequency of 10 Hz. Values are such that any meaningful laboratory measurement is not likely, because the dimensions associated with an experiment require hundreds of kilometers to achieve a detectable change. The marine environment is so variable over these dimensions that cause and effect are blended.

Problems associated with understanding the acoustic properties of sediments have many similarities. At the time the work discussed here was published [*Hampton*, 1967], it represented the widest range of frequencies examined in a systematic fashion to that time. Seawater as an acoustic medium has a relatively narrow range of variability when compared to naturally occurring sediments. One of the challenges in studying acoustic properties of sediments is not only determining what parameters are significant, but then measuring those parameters to the necessary accuracy. Guidance for selecting significant parameters could best come from a good analytical description. Although progress has been made on an analytical description, there are still many unanswered questions, primarily because of the wide range and variability of the parameters involved.

This paper will not address all the areas of interest in studying the behavior of sound in sediments. Some of the more interesting current problems will be addressed in the final sections. The focus of the work described in this paper will be low-frequency, long-range propagation. Aspects of the problem are illustrated in Figure 1, which shows received SUS (SUS is the military designator for Signal, Underwater Sound and is a widely used 1.8-lb (~0.8 kg) explosive device with a hydrostatic fuse) waveforms for three oceans. The bandwidth is from 10 to 500 Hz. For all three cases, all of the energy, with the exception of the first arrival, is via bottom-interacting paths. It is obvious that for any prediction capability (i.e., ability to accurately describe the behavior by means of a suitable analytical description) the acoustic properties of the bottom must be known.

This paper reviews the work of *Hampton* [1967] and gives one example of the extension of that work to lower frequencies. The paper concludes with a summary of the progress of applying the Biot-Stoll model to the experimental results.

LABORATORY MEASUREMENTS

Following is a brief review of the laboratory measurements, made at Applied Research Laboratories, The University of Texas at Austin (ARL:UT) by *Hampton* [1967]; Figures 2–6 are taken from that paper. No discussion of measurement techniques will be repeated here; they are given in that paper. Figure 2 begins with a summary of the measurements of sediment attenuation. The vertical scale is attenuation in decibels per foot (the scales used in the original 1967 publication are retained), and the horizontal scale is frequency in kilohertz. Measurement results are shown for kaolinite and Black Sediment. The number in parentheses following the sediment description is the value of sediment concentration for that measurement. The probe method covered the frequency range of 50–600 kHz with a measurement limitation of about 2 dB/ft (6.6 dB/m). The frequency range of 4–30 kHz was measured using standing wave tube techniques and extended the sensitivity of the measurements down to between 0.05 and 0.1 dB/ft (0.165 and 0.33 dB/m). The accepted values of attenuation in water and seawater are shown in Figure 2 for comparison, and it should be noted that the difference is between two and four orders of magnitude.

One set of measurements overlapped the probe and tube techniques, the curve labeled large sample measurements. These measurements were made using the probe technique,

Paper number 4R1326.
8755-1209/85/004R-1326$15.00

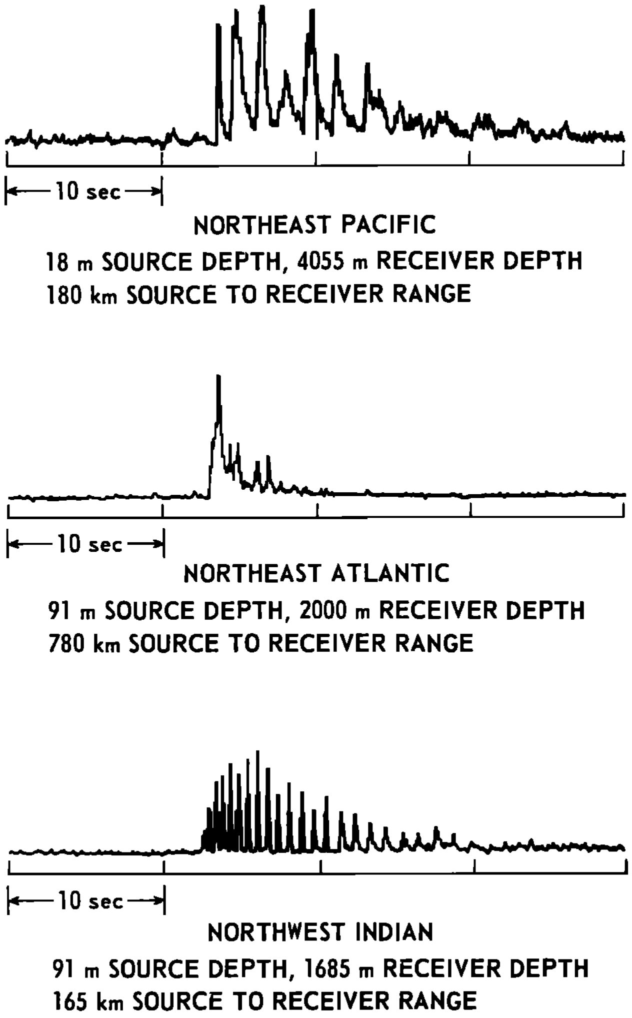

Fig. 1. Received SUS waveform: 10- to 500-Hz bandwidth.

but were made using a container that allowed approximately 10 times the test distance used previously and thus improved the sensitivity at low values of attenuation.

For both the Black Sediment and the kaolinite at concentrations which are essentially stable (i.e., the sediment has set long enough that the rate of change of concentration has become very small), the frequency dependence of the attenuation is $f^{1.37}$, with the actual value having some dependence on value of concentration. The dependence on concentration is shown over a wider range in Figure 3. Measurements are shown for 0.03, 12, 20, 30, and 37% concentration. For these measurements the maximum value of attenuation occurs at 20%, with much lower values at both 0.03 and 37%.

Figure 3 also shows that a factor other than concentration is making a contribution. In the low-frequency range, for concentrations near 30%, measurements are shown for undispersed (i.e., the case where the sediment is allowed to settle naturally) and for dispersed, the case where a small amount of wetting agent has been added. For these two cases, there is a significant change in attenuation value and in frequency dependence. As will be seen later, the frequency dependence for the undispersed case is quite similar to that of sands.

Figure 4 repeats some of the Black Sediment and kaolinite data and examines sand mixtures. For the mixtures, the first number shown on the curve is the amount of sand by percent, and the second number is the concentration of the mixture. As the amount of sand is increased, the attenuation increases, and the frequency dependence changes as well.

Figure 5 gives results for several sands (the ϕ scale is a measure of the sand particle diameter, where $\phi = -\log_2$ diameter (mm)). One kaolinite and one kaolinite with 30% sand measurement are repeated for comparison. The work by Nolle et al. was published in 1963. The frequency dependence is close to the $f^{0.5}$ from *Nolle et al.* [1963], but the agreement with the measurements shown here is not adequate to rule out other frequency effects.

Figure 6 shows the results of acoustic velocity measurements for kaolinite and Black Sediment. Although the dispersion is small (4% or less over about two frequency decades), it is predicted by the Kramers-Kronig dispersion relationship from the measured values of attenuation [*Horton*, 1974]. The bandwidth of the measurements played an important role in establishing the dispersion.

The measurements summarized in these five figures were of value, but they did not result in a useful analytical model. In fact, they caused a modest controversy because they contradicted the results obtained using a simple linear viscoelastic model [*Hamilton*, 1974] which predicted a first power of frequency dependence of attenuation. An important question was whether or not the frequency dependence from this work, which varied about $f^{1.0}$ (i.e., $f^{1.37}$ for clays to $f^{0.5}$ for sands), was a result of using laboratory sediments and would be different for natural sediments. The assumption by Hamilton of $f^{1.0}$ was supported by a summary of all published values from natural sediments; however, almost all were made at a single frequency or over a narrow frequency range. The values of attenuation reported here were consistent with the range of values analyzed by *Hamilton* [1974]. The critical issue remained the large difference in values of attenuation upon extrapolation to low (10–100 Hz) frequencies using the two frequency effects.

Stoll [1974] examined the potential for applying the Biot theory to saturated sediments, and the application later became known as the Biot-Stoll theory. In his 1974 work he concluded that the Biot theory had the potential for describing the frequency effects summarized above, but required experimental data below 10 kHz to evaluate the usefulness. The next section describes one method that was used to get the low-frequency values of velocity and attenuation.

LOW-FREQUENCY IN SITU MEASUREMENTS

This section describes a method that uses impulsive acoustic sources (in this case a 1.8-lb explosive charge called a SUS) and, by accurate reconstruction of the history of the multiple arrivals from the source, extracts attenuation values for the sediment path. Because the impulsive source is broadband, values are obtained from 25 Hz to 400 Hz. Before this method was developed, the usefulness of SUS had been criticized. Criticism of SUS centered on the failure of the SUS to achieve consistent results in propagation measurements. As the results discussed here will show, this failure was due primarily to analysis techniques that examined the total energy of the received signal. The method described here incorporated the prediction capability of an eigenray model that had sufficient accuracy to reconstruct all significant transmission paths. Some aspects of the technique were demonstrated in an analysis of signal speed in long-range propagation [*Mitchell and Hampton*, 1978]. The technique is fully documented (to its

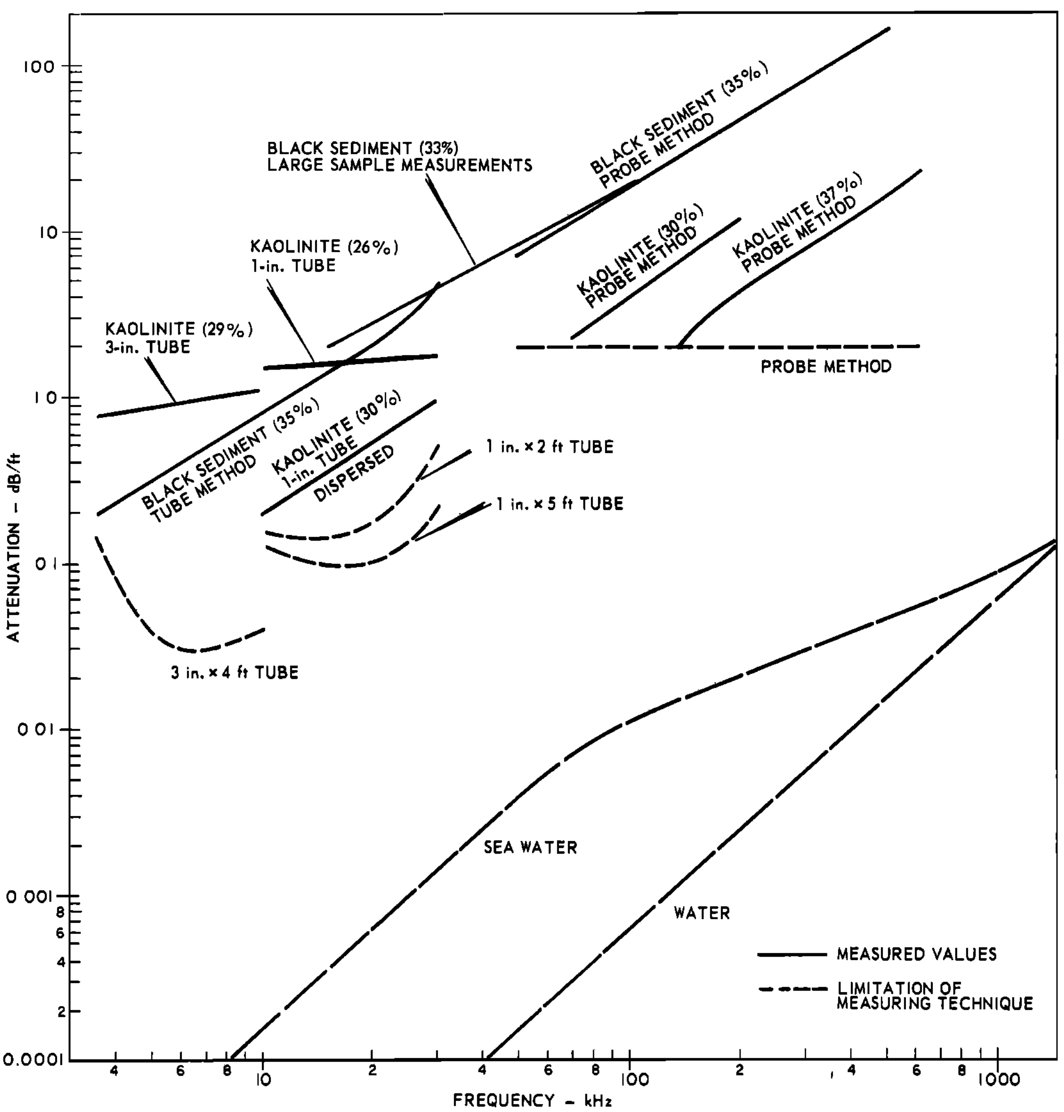

Fig. 2. Summary of ARL:UT sediment attenuation measurements.

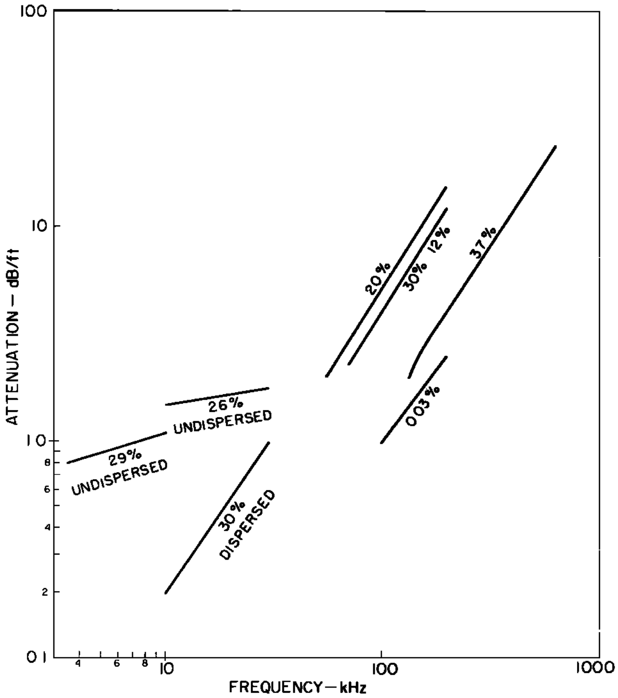

Fig. 3. Kaolinite: attenuation versus frequency at several concentrations.

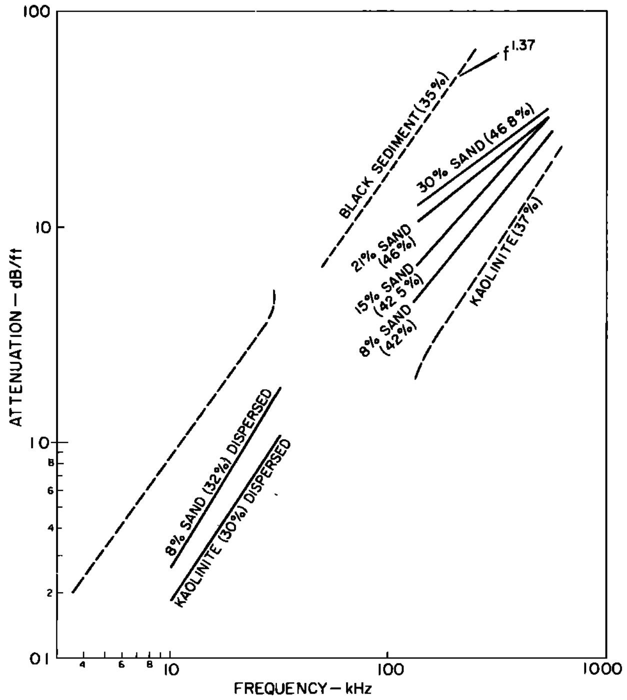

Fig. 4. Kaolinite and sand: attenuation versus frequency.

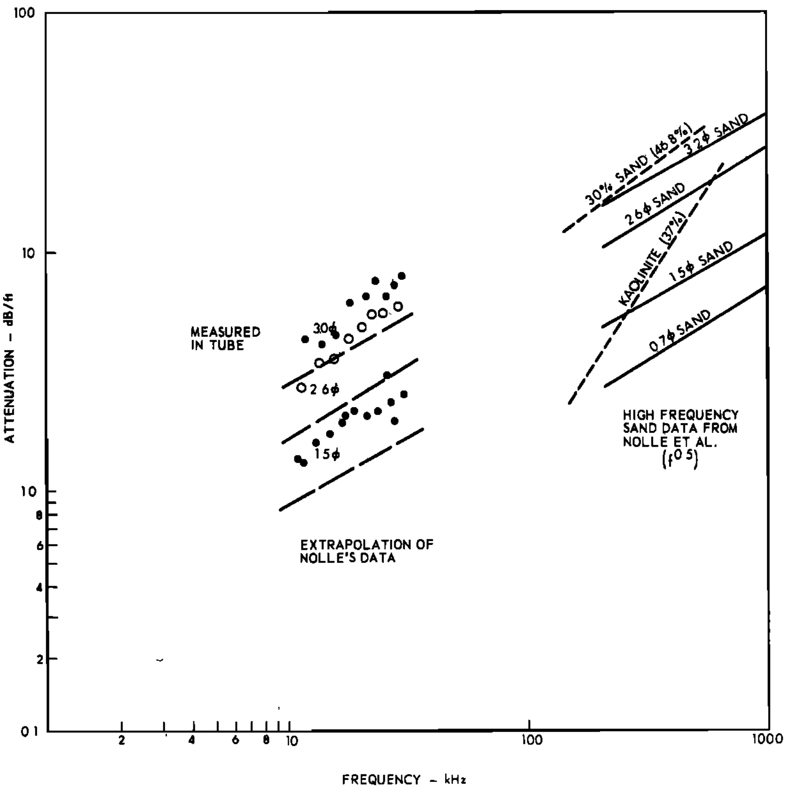

Fig. 5. Attenuation versus frequency for sand.

current state) by *Hampton et al.* [1978], *Mitchell et al.* [1980], and *Mitchell and Focke* [1980].

The data used are illustrated in Figure 7, which shows six SUS arrival envelopes. The measurements are made by placing a series of receivers vertically in the water column (the data shown are from the receiver located at 1685 m) and dropping SUS charges along a path with a SUS separation selected to give a useful data density. These six envelopes with a transmission range near 80 km are for range differences of about 1 km. SUS are designed to detonate at selected depths, and three depths are shown here: 245, 91, and 18 m. Some of the differences in the arrival envelopes are significant; the 18-m SUS couples less energy to the 1685-m receiver, and the 91-m SUS has less energy in the early arrivals. The sequence is also labeled by SUS number and by date/time group. For the two 91-m SUS envelopes, particular arrivals have been labeled

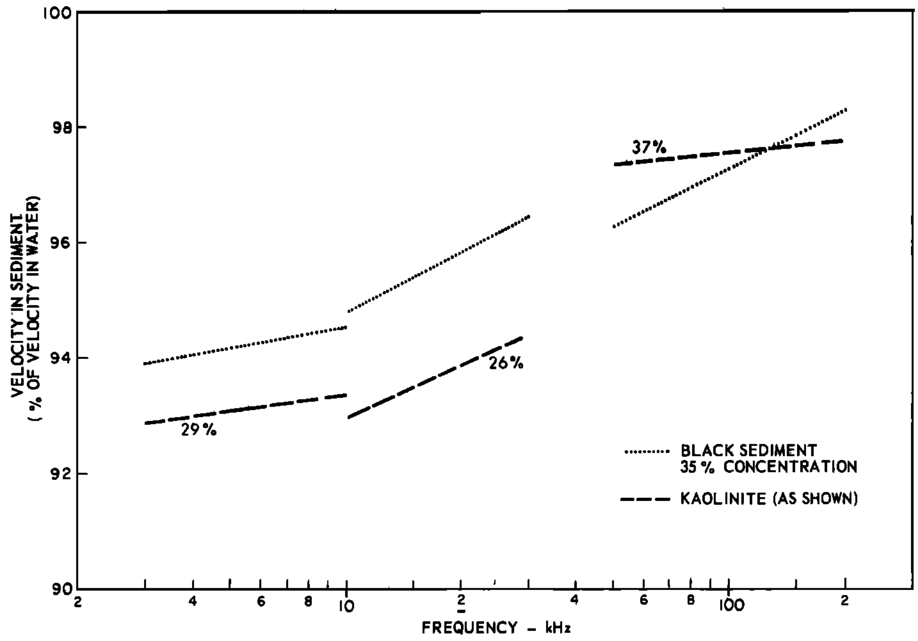

Fig. 6. Summary of ARL:UT sediment-velocity measurements.

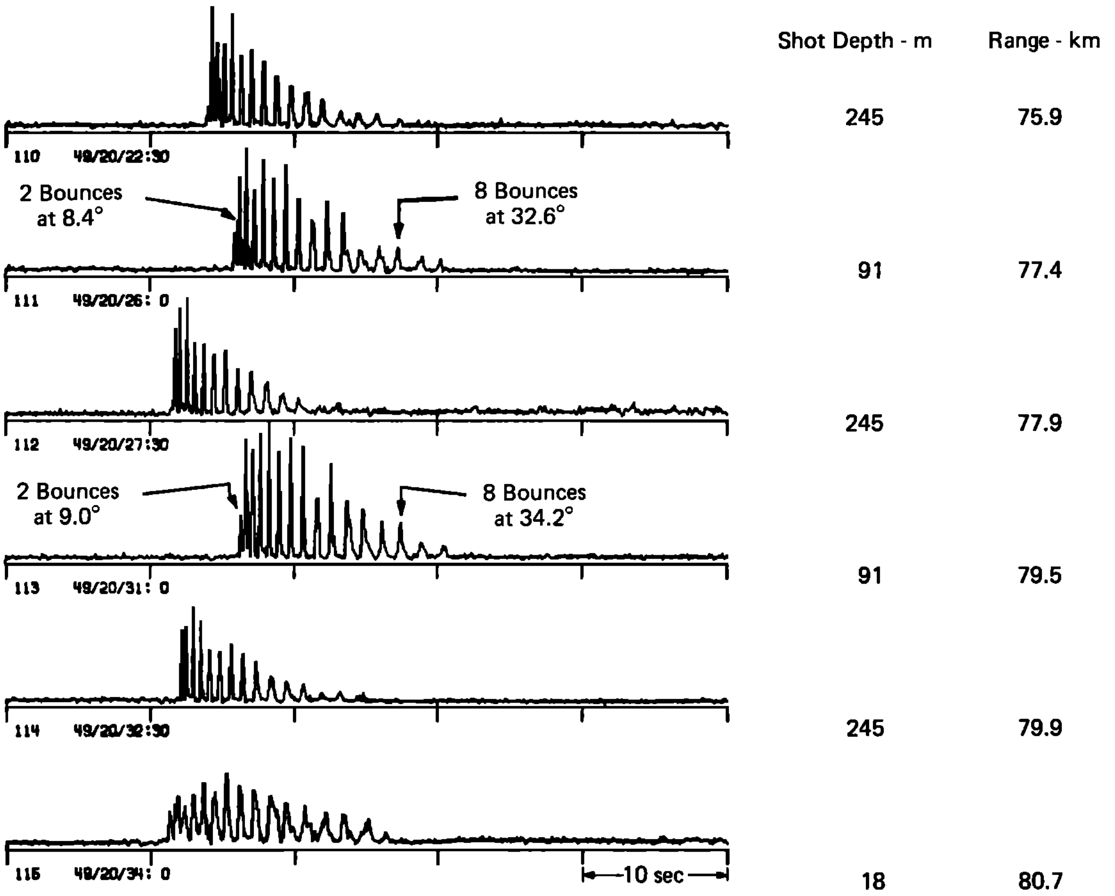

Fig. 7. SUS arrival envelopes: 1685-m receiver.

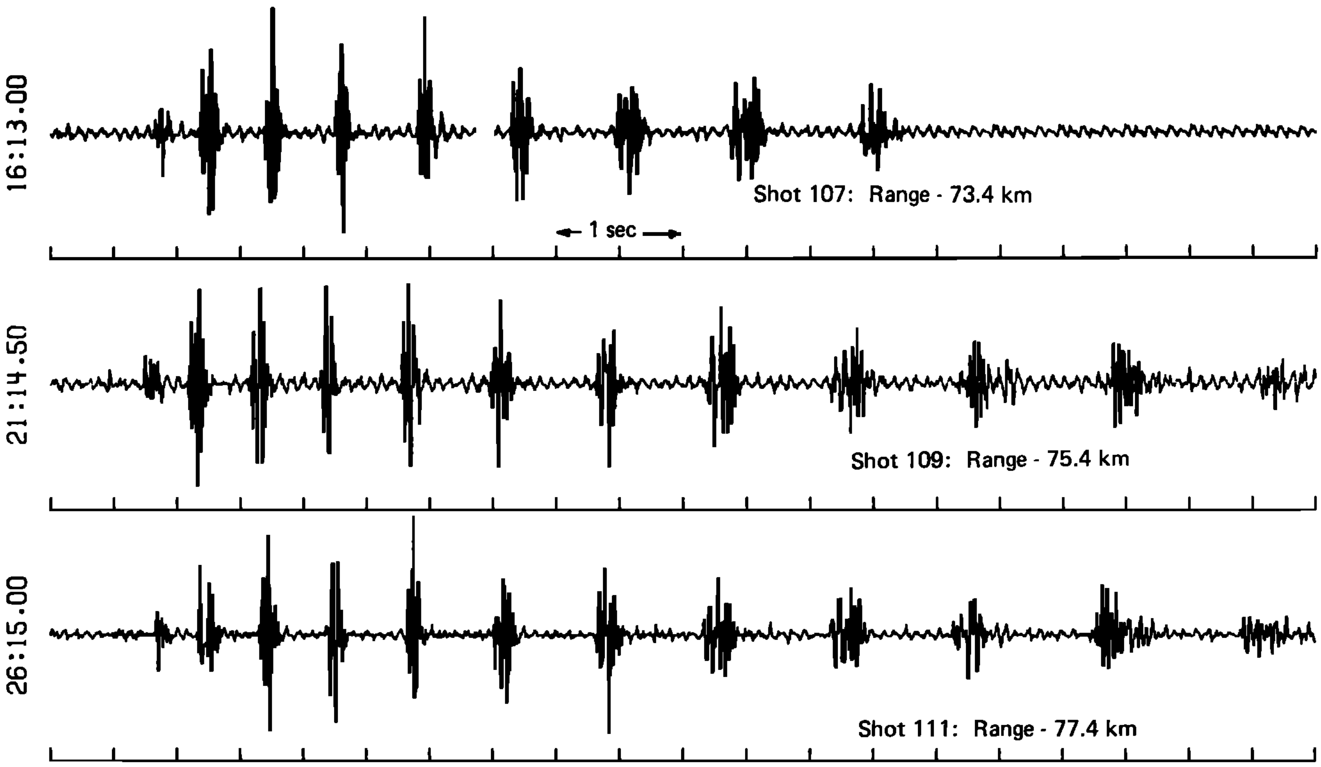

Fig. 8. SUS high-resolution plots: 1685-m receiver, 91-m shots, 10- to 50-Hz band.

Ray Index	Ray Direction at Source/Receiver	Travel Time - sec	Speed	Bottom Angle	Bottom Reflections	Surface Angle	Surface Reflections	Phase Velocity	Pressure**
1	↓ ↓	55.155	1479.44	7.82D	2	*	2	1529	2.35E-05
2	↓ ↓	55.160	1479.32	8.91D	2	2.77D	2	1533	1.14E-05
3	↑ ↓	55.155	1479.44	7.84D	2	*	3	1529	2.25E-05
4	↑ ↓	55.153	1479.50	8.54D	2	*	3	1531	5.74E-06
5	↑ ↓	55.166	1479.14	9.16D	2	3.49D	3	1534	1.19E-05
6	↓ ↑	55.623	1466.99	10.90D	3	6.89D	2	1542	1.40E-05
7	↑ ↑	55.638	1466.61	11.14D	3	7.26D	3	1543	1.37E-05
8	↓ ↓	56.157	1453.06	13.38D	3	10.39D	3	1557	1.32E-05
9	↑ ↓	56.178	1452.50	13.56D	3	10.63D	4	1558	1.31E-05
10	↓ ↑	56.773	1437.28	15.70D	4	13.26D	3	1573	1.28E-05
11	↑ ↑	56.801	1436.58	15.86D	4	13.46D	4	1574	1.27E-05
12	↓ ↓	57.469	1419.89	18.00D	4	15.94D	4	1592	1.24E-05
13	↑ ↓	57.502	1419.08	18.15D	4	16.11D	5	1594	1.23E-05
14	↓ ↑	58.239	1401.11	20.17D	5	18.37D	4	1613	1.21E-05
15	↑ ↑	58.277	1400.20	20.31D	5	18.53D	5	1615	1.21E-05
16	↓ ↓	59.086	1381.02	22.31D	5	20.71D	5	1637	1.18E-05
17	↑ ↓	59.128	1380.03	22.43D	5	20.85D	6	1638	1.18E-05
18	↓ ↑	60.000	1359.99	24.33D	6	22.89D	5	1662	1.16E-05
19	↑ ↑	60.046	1358.94	24.45D	6	23.02D	6	1664	1.16E-05
20	↓ ↓	60.987	1337.98	26.31D	6	25.00D	6	1689	1.13E-05
21	↑ ↓	61.037	1336.88	26.42D	6	25.12D	7	1691	1.13E-05
22	↓ ↑	62.031	1315.45	28.19D	7	26.99D	6	1718	1.11E-05
23	↑ ↑	62.085	1314.31	28.30D	7	27.10D	7	1720	1.11E-05
24	↓ ↓	63.145	1292.25	30.02D	7	28.91D	7	1749	1.09E-05
25	↑ ↓	63.202	1291.08	30.13D	7	29.02D	8	1751	1.09E-05
26	↓ ↑	64.308	1268.88	31.76D	8	30.73D	7	1781	1.07E-05
27	↑ ↑	64.369	1267.69	31.86D	8	30.83D	8	1783	1.07E-05
28	↓ ↓	65.535	1245.11	33.46D	8	32.49D	8	1815	1.04E-05
29	↑ ↓	65.599	1243.90	33.56D	8	32.59D	9	1817	1.04E-05

*Upper Refractions
**Relative to 1 yd

Fig. 9. Ray trace computations for 91-m shot 111 at 77.4-km range: 1865-m receiver.

according to number of bottom interactions (i.e., "bounces") and bottom interaction angle. The next few figures illustrate the method used to determine this information about each arrival. Figure 8 shows more detail for three 91-m SUS arrivals plotted with a bandwidth of 10–50 Hz. This resolution is necessary to begin to observe the variability in arrival multipath spacing for changes of 2 km in a 75-km range.

The first step in reconstructing the history of each arrival is

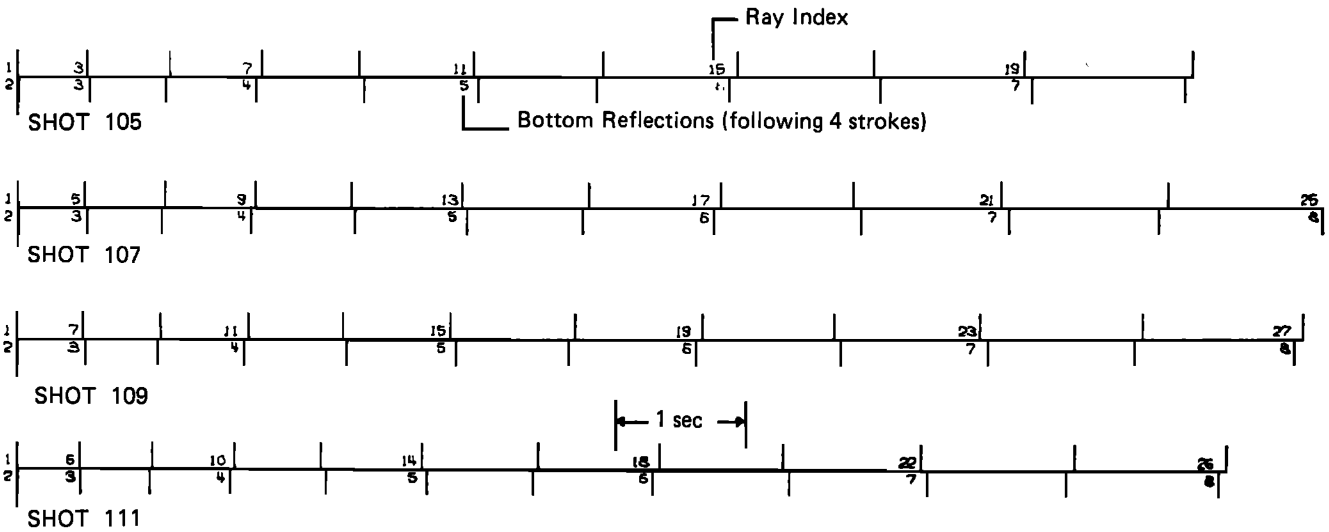

Fig. 10. Ray trace arrival structure plots for 91-m shots: 1685-m receiver. (Up/down stroke denotes an arrival with odd/even surface reflections.)

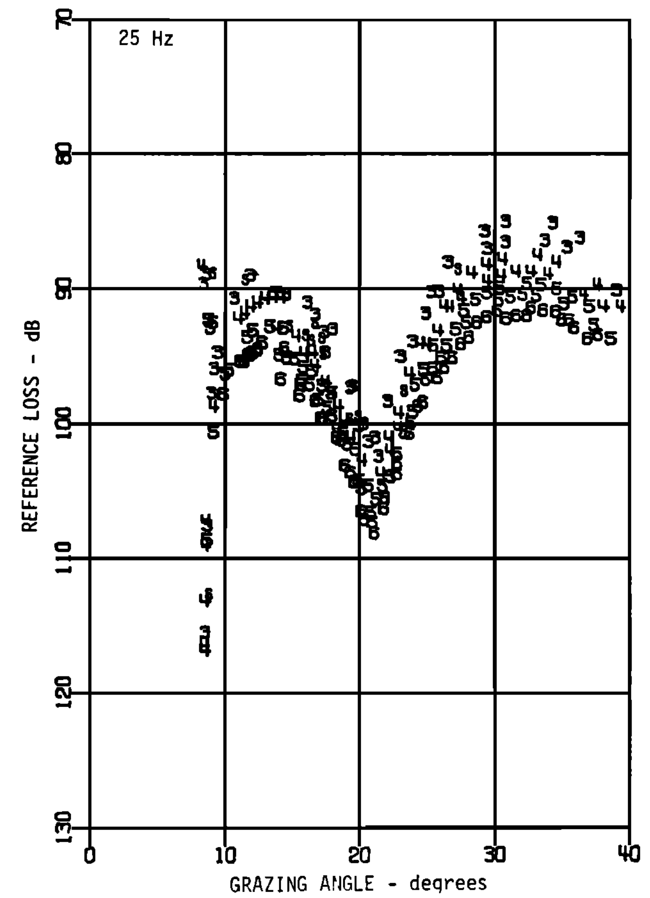

Fig. 11. Reference propagation loss versus grazing angle: 1685-m receiver; 91-m SUS; 25 Hz.

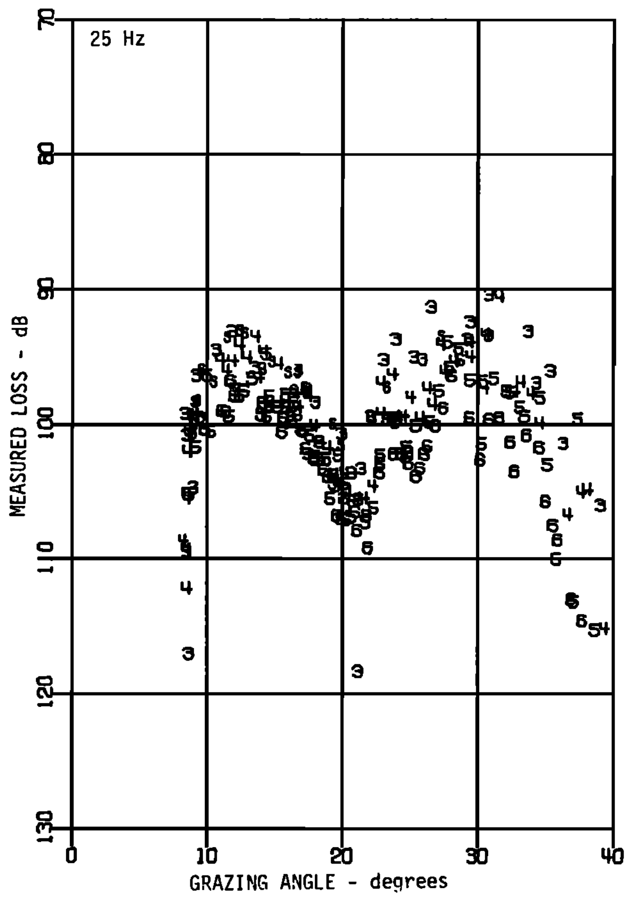

Fig. 12. Measured propagation loss versus grazing angle: 1685-m receiver; 91-m SUS; 25 Hz.

to use an eigenray "model" to obtain details of all rays possible for the geometry and environment. A sample result is shown in Figure 9. For this example, 29 rays are possible. For the case shown in Figure 9 there are three surface-refracting rays (marked with an asterisk), but there are no bottom-refracting rays; the minimum bottom angle is 7.8°. The column labeled pressure is a simple spreading loss accounting of the energy, assuming no loss in the bottom. These computations assume that bathymetry and sound velocity structure do not vary with range; for the example used here these are good assumptions. Within a selected interval, usually 10 or 20 s, all of the eigenrays are determined to within 1 m in range. That is, the root-finding iterations to find each ray are terminated when a ray is found which leaves the source and passes through the receiver depth at a range within 1 m of the source range. Thus the signal travel time along each ray is determined to better than 1 ms.

The computations of Figure 9 are coded into a time sequence to allow comparison with the SUS data. Figure 10 is an example of the coding method and includes timing information along with details of surface and bottom reflections. In the analysis process, the only manual step necessary is the comparison of information illustrated in Figures 8 and 10 to verify that the modeled arrival structure is adequate to represent the measurement and to correct for timing errors due to, for example, detonation time uncertainties.

The method of extracting bottom loss from the data is illustrated in the next three figures. The reference propagation loss which is obtained by the eigenray calculations (last column of Figure 9) is plotted versus bottom grazing angle (fourth column of Figure 9) and is coded according to number of bottom reflections (fifth column of Figure 9) (i.e., 3 represents three bottom reflections, etc.). These calculated results are

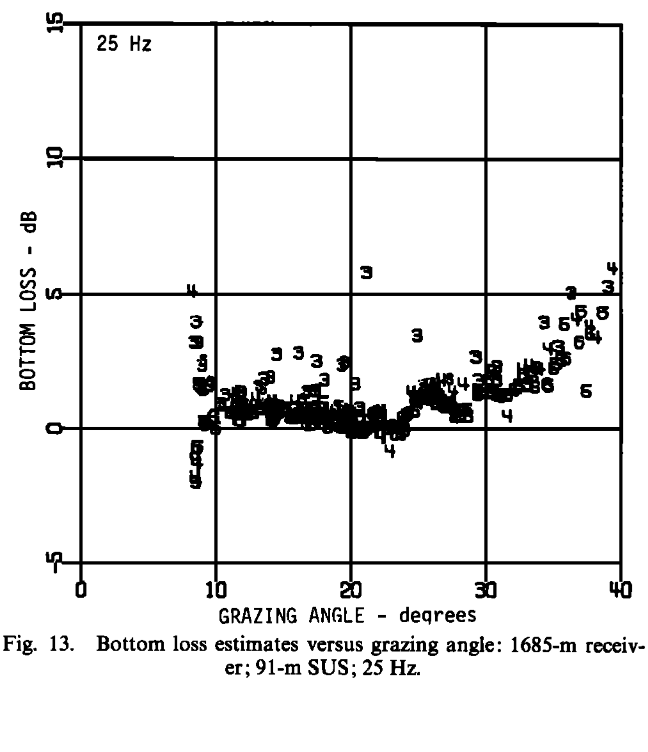

Fig. 13. Bottom loss estimates versus grazing angle: 1685-m receiver; 91-m SUS; 25 Hz.

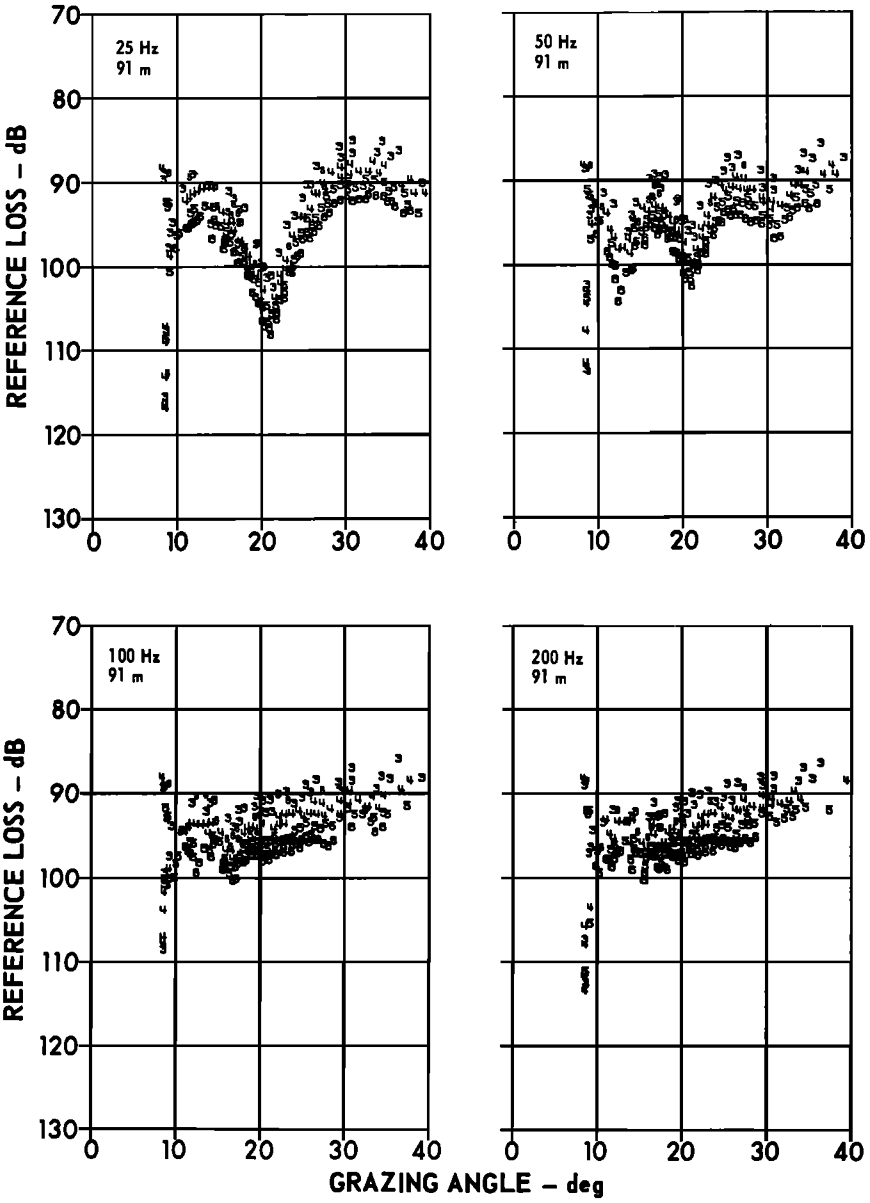

Fig. 14. Reference propagation loss versus grazing angle: 1685-m receiver; 91-m SUS; 25, 50, 100, 200 Hz.

shown for 25 Hz in Figure 11 and are plotted against grazing angle in degrees. The reference propagation loss is computed by summing the contributions of the rays within the time interval and averaging over the one or one-third octave bands used. Figure 11 illustrates the necessity of combining the signal components coherently. The null near 20° is caused by surface image interference (also known as Lloyd's mirror effect or surface decoupling). Subsequent examples will show the frequency dependence of these effects (the source depth dependence is shown by *Mitchell et al.* [1980]). This method of presenting the data also shows that the strongest arrivals are not always those at the lowest grazing angles.

The measured arrival propagation loss plotted versus grazing angle for this case is shown in Figure 12, and the surface image interference is seen as the dominant effect in the received signals. From the information illustrated in these two figures, bottom loss versus grazing angle can be extracted. On a point by point basis, the measured propagation loss is compared to the reference propagation, and the difference is normalized by the number of bottom interactions. The result for this case is shown in Figure 13. Several features of these results are of special interest. Perhaps most important are the small values and in addition the small spread in values from such a large number of data points (approximately 500 for this example). Also, the surface image interference effect which dominates the propagation loss data is no longer present. More detailed analysis from other source and receiver depths [*Mitchell et al.*, 1980] shows the variation beginning at about 24° to be a repeatable effect. Values are not given for grazing angles below about 8° because, as shown in Figure 9, for this bottom-limited region there are no bottom-interacting paths at lower grazing angles.

The next three figures (Figures 14–16) repeat this same sequence, but give details for four frequencies, 25, 50, 100, and 200 Hz. This illustrates the frequency effects of the surface image interference and also the increased value of bottom loss as frequency increases and as grazing angle increases.

The method used to transform bottom loss data to bottom

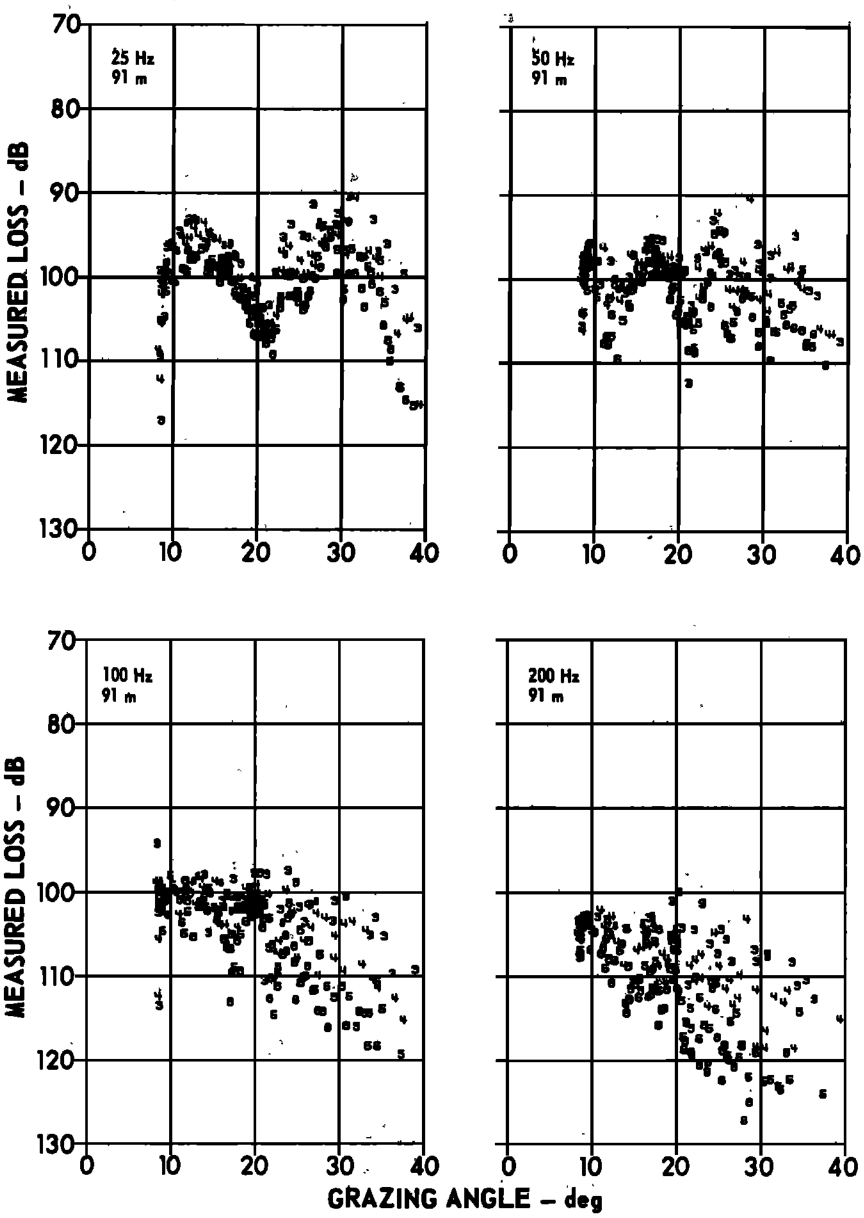

Fig. 15. Measured propagation loss versus grazing angle: 1685-m receiver; 91-m SUS; 25, 50, 100, 200 Hz.

attenuation profiles is documented in detail by *Mitchell and Focke* [1980]. Based on a reasonable model of bottom reflection, the bottom loss behavior with grazing angle can be divided into two major effects: loss contribution from bottom-penetrating ray paths and the Rayleigh reflection limit. With suitable assumptions an iterative technique can then be applied to invert the bottom loss curve to a bottom attenuation profile. An example of the results is shown in Figure 17, which shows attenuation profiles representative of several basin regions.

INTERPRETATION OF RESULTS

For reasons explained in *Mitchell and Focke*'s [1980] paper, attenuation shown in Figure 17 is presented in units of decibels per meter–kilohertz. These measurements are of effective attenuation from all causes, intrinsic absorption, scattering, and reflection, and for these results are based on an f^1 frequency dependence. To date, studies of correlations between attenuation and sediment types or geographic regions have not been completed. However, for the examples shown in Figure 17 it is known that the profiles labeled low (L) and medium (M) attenuation are from regions with silty clay or clayey silt terrigenous sediments which have turbidite layering. The profile labeled high (H) attenuation is from a region with silty turbidite layers in a calcareous ooze/calcareous clay sediment. *Hamilton* [1976] extended his analysis of ocean sediment attenuation and particularly addressed the depth dependence. It is of value to make a comparison of Figure 17 presented here and Figure 1 from the *Hamilton* [1976] paper. Both involved basin regions, and a comparison is justified. In general, the values of attenuation presented in Figure 17 are an order of magnitude smaller than the values of the *Hamilton* [1976] paper.

A final comparison is of interest; *Hovem and Ingram* [1979]

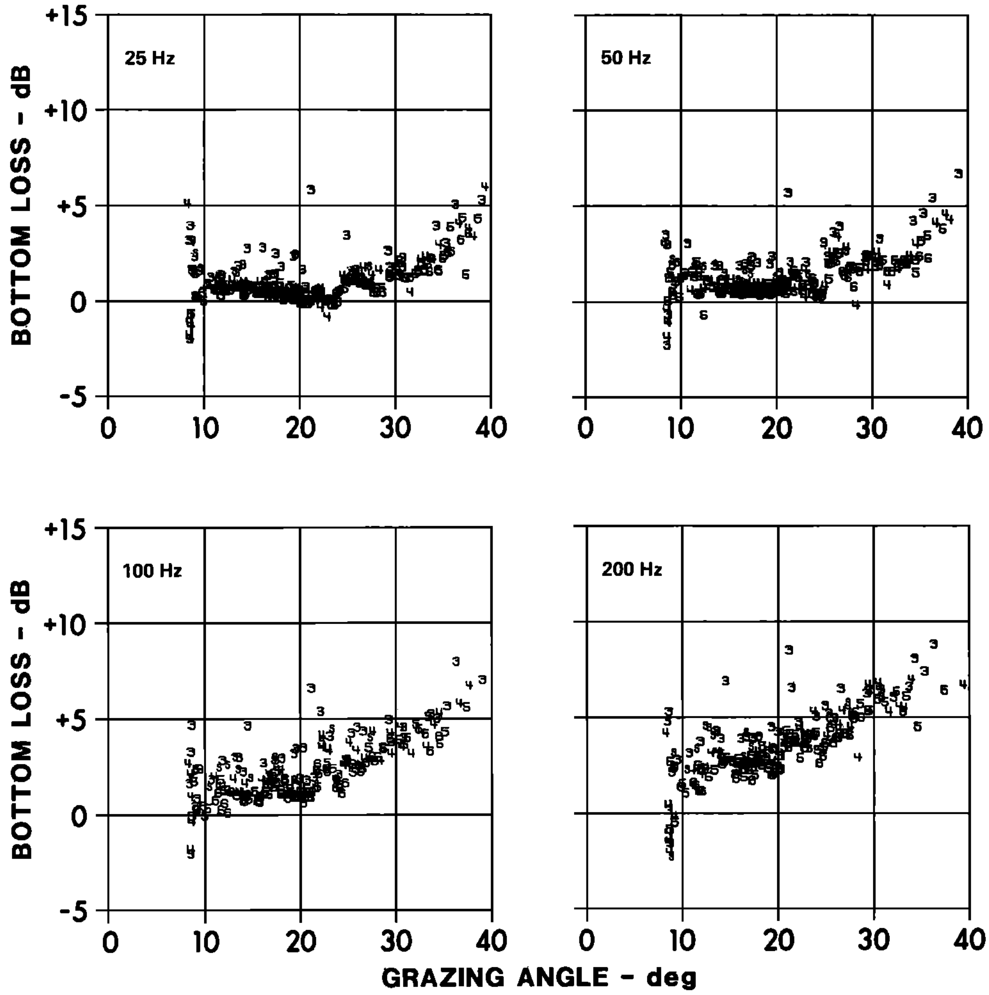

Fig. 16. Bottom loss estimates versus grazing angle: 1685-m receiver; 91-m SUS; 25, 50, 100, 200 Hz.

and *Hovem* [1980] extended the earlier work of the Biot theory (now commonly called the Biot-Stoll theory). Although the Biot-Stoll theory is applied to sands, silts, and clays, the significant physical parameters and the dominant physical mechanisms differ for different components and frequencies. *Bedford* [1982] goes into detail on some of these differences, and he discusses the emphasis of the work of *Stoll* [1974] and of *Hovem* [1980]. *Hovem and Ingram* [1979] examine saturated sands and show viscous attenuation to be the dominant factor. Viscous attenuation will show an f^2 dependence at low frequencies and $f^{1/2}$ at high frequencies. The transition between these two dependences is in the range of 100 Hz to 10 kHz, depending on grain size. Figure 18 shows in detail a comparison of theoretical viscous attenuation effects and the sand measurements discussed previously in Figure 5. The agreement is quite encouraging, but perhaps more revealing is the theoretical viscous attenuation over a wider frequency range, as shown in Figure 19. Also shown in Figure 19 is the compilation from *Hamilton* [1972] and a comparison of a simple linear extrapolation with the theoretical predictions. No low-frequency data exist for sand, and an important question remains as to the validity of these low-frequency predictions.

Figure 20, which is taken from *Hovem* [1980], shows the compressional wave attenuation as a function of frequency for the Black Sediment discussed previously. As appropriate for this sediment, Hovem has used the Biot-Stoll theory and what he terms a modified suspension theory, and these are compared to the measurements reported by *Hampton* [1967]. It is appropriate to attempt a comparison with the recent low-frequency results summarized in Figure 17; however, the comparison must be made with some caution. The Black Sediment is grossly characterized as a silty-clay, which is consistent with the gross characterization for the low- and medium-attenuation profiles of Figure 17. With this as justification, the results of Figure 17 are placed in Figure 20. The maximum range at the water-sediment interface (i.e., 0.005 to 0.027 dB/m-kHz) is shown as the vertical extent, and the shaded portion extends from 25 Hz to 400 Hz, the frequency range covered in the analysis. The analysis [*Mitchell and Focke*, 1980] that resulted in Figure 17 assumed an $f^{1.0}$ frequency dependence, and that is shown here. The results would be modified to some degree with the assumption of a different frequency dependence, but that has not been done. It is further worth noting that any problems with noise contamination of the data, especially at the low values of attenuation (i.e., low frequencies), result in values of attenuation that are high. With these two factors considered, the agreement with the Biot theory would improve; however, the agreement is considered encouraging as presented here.

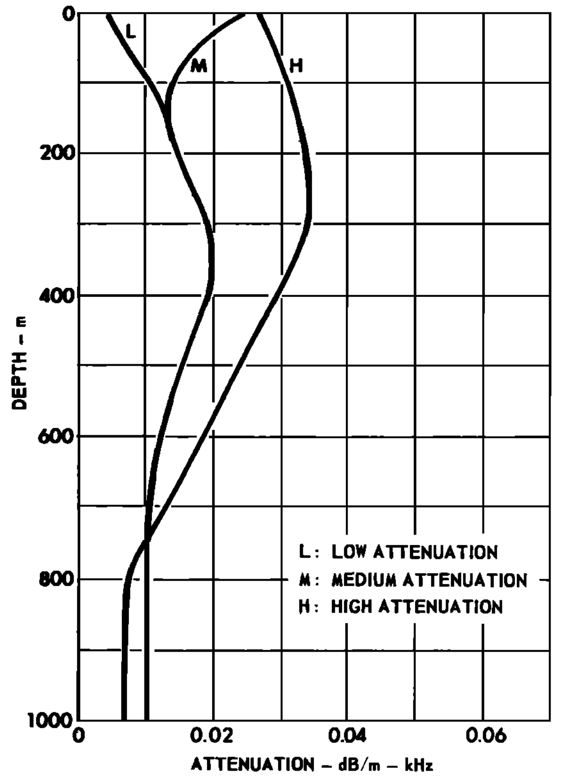

Fig. 17. Attenuation profiles representative of several basin regions.

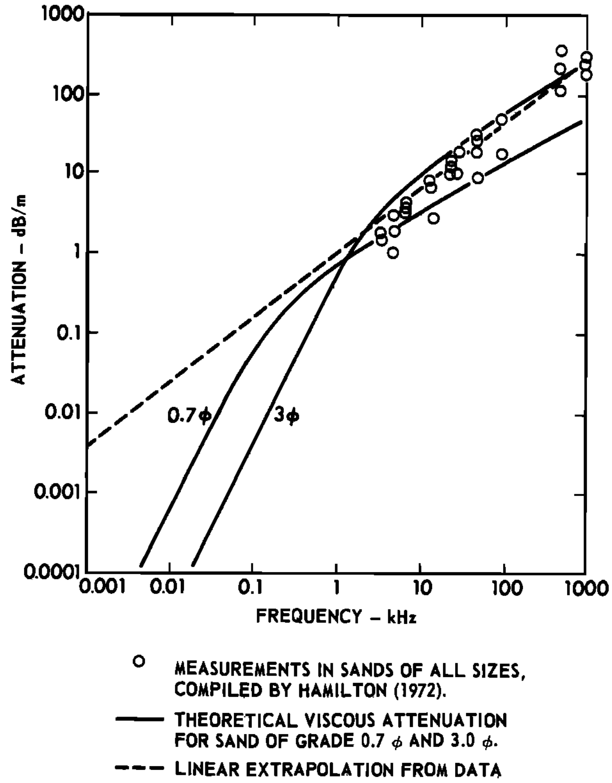

Fig. 19. Viscous attenuation of compressional waves in sand.

PROJECTIONS FOR THE FUTURE

The desirable goal of making simple measurements on a small sample in the laboratory and predicting its in situ acoustic properties, especially at low frequency, has not been achieved. Several important considerations are given below.

1. The successful analysis of the individual arrivals from an explosive source (SUS) has restored the measurement method to its important position as an inexpensive and useful measurement technique.

2. The low values of bottom sediment attenuation which have successfully explained acoustic propagation effects (including high noise levels that had not been previously understood) have alerted us to the difficult problem of in situ measurement of those values.

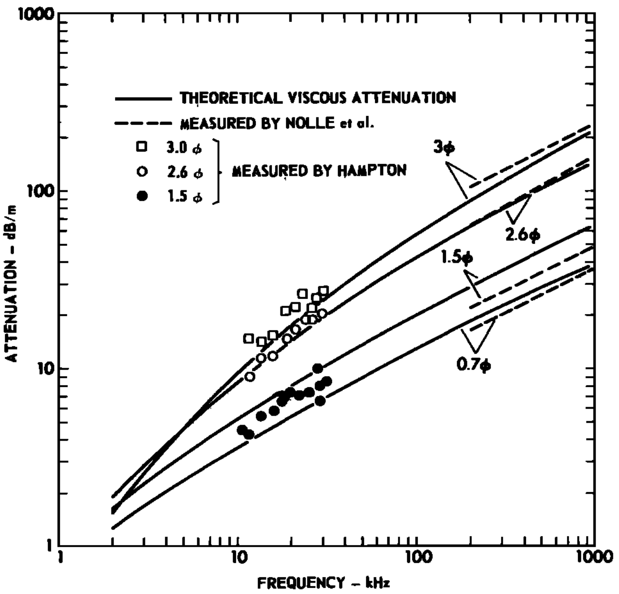

Fig. 18. Compressional wave attenuation as a function of frequency for water-saturated sands.

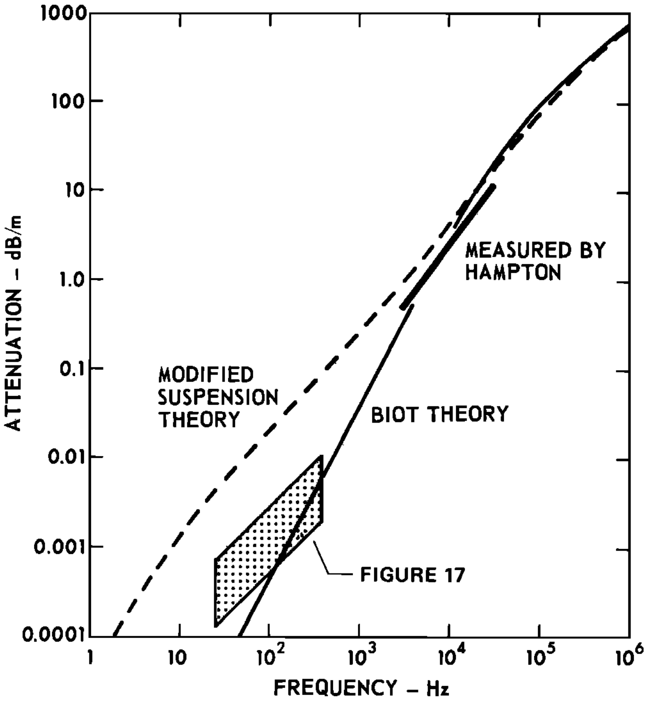

Fig. 20. Compressional wave attenuation as a function of frequency for a black soil sediment.

3. The analysis of in situ measurements discussed here included assumptions of sediment thickness and homogeneity that cannot always be met. An important consideration is what modifications are necessary to study more complex environments. For cases involving thin sediments, a critical issue is the effect of subbottom scattering.

4. No discussion of shear waves is given here. For many important sediment conditions, the shear wave parameters may be good indicators of acoustic wave parameters, and further study is required.

Acknowledgments. The purpose of this paper is to present and comment on a particular area of progress: understanding acoustic properties of sediments. The author has been involved in a limited way in some of the work. Every effort is made in the paper to carefully acknowledge that the work of many people is discussed.

REFERENCES

Bedford, A., On the current status of theoretical modeling of acoustic waves in saturated sediments, *Tech. Rep. ARL-TR-82-32*, Appl. Res. Lab., Univ. of Tex. at Austin, June 1982.

Hamilton, E. L., Compressional-wave attenuation in marine sediments, *Geophysics, 37*, 620–646, 1972.

Hamilton, E. L., Geoacoustic models of the sea floor, in *Physics of Sound in Marine Sediments*, edited by L. D. Hampton, pp. 181–221, Plenum, New York, 1974.

Hamilton, E. L., Sound attenuation as a function of depth in the sea floor, *J. Acoust. Soc. Am., 59*, 528–535, 1976.

Hampton, L. D., Acoustic properties of sediments, *J. Acoust. Soc. Am., 42*(4), 882–890, 1967.

Hampton, L. D., S. K. Mitchell, and R. R. Gardner, Acoustic bottom loss measurement using multipath resolution, in *Proceedings of the EASCON 78 IEEE Meeting, Washington, D.C., 24–27 September 1978*, pp. 235–251, Institute of Electrical and Electronics Engineers, New York, 1978.

Horton, C. W., Sr., Dispersion relationships in sediments and seawater, *J. Acoust. Soc. Am., 55*(3), 547–549, 1974.

Hovem, J. M., Viscous attenuation of sound in suspensions and high-porosity marine sediments, *J. Acoust. Soc. Am., 67*(5), 1559–1563, 1980.

Hovem, J. M., and G. D. Ingram, Viscous attenuation of sound in saturated sand, *J. Acoust. Soc. Am., 66*(6), 1807–1812, 1979.

Mitchell, S. K., and K. C. Focke, New measurements of compressional wave attenuation in deep ocean sediments, *J. Acoust. Soc. Am., 67*(5), 1582–1589, 1980.

Mitchell, S. K., and L. D. Hampton, Signal speed in long-range propagation, *J. Acoust. Soc. Am., 63*(2), 386–390, 1978.

Mitchell, S. K., N. R. Bedford, and G. E. Ellis, Multipath analysis of explosive source signals in the ocean, *J. Acoust. Soc. Am., 67*(5), 1590–1597, 1980.

Nolle, A. W., W. A. Hoyer, J. F. Mifsud, W. R. Runyan, and M. B. Ward, Acoustical properties of water-filled sands, *J. Acoust. Soc. Am., 35*, 1394–1408, 1963.

Stoll, R. D., Acoustic waves in saturated sediments, in *Physics of Sound in Marine Sediments*, edited by L. D. Hampton, pp. 19–39, Plenum, New York, 1974.

L. D. Hampton, Applied Research Laboratories, The University of Texas at Austin, Austin, TX 78713.

(Received October 25, 1984;
accepted October 29, 1984.)